THE ASTROPHYSICAL JOURNAL, 376:266–271, 1991 July 20

TOMOGRAPHIC SEPARATION OF COMPOSITE SPECTRA: THE COMPONENTS OF THE O-STAR SPECTROSCOPIC BINARY AO CASSIOPEIAE

WILLIAM G. BAGNUOLO, JR., AND DOUGLAS R. GIES
Center for High Angular Resolution Astronomy, Department of Physics and Astronomy, Georgia State University, Atlanta, GA 30303
Received 1990 November 20; accepted 1991 January 15

ABSTRACT

We have analyzed the UV photospheric lines of the short-period, double-lined O-star spectroscopic binary AO Cas. Archival data from *IUE* (16 spectra uniformly distributed in orbital phase) were analyzed with a tomography algorithm to produce the separate spectra of the two stars in six spectral regions. The spectral classifications of the primary and secondary, O9.5 III and O8 V, respectively, were estimated through a comparison of UV line ratios with those in spectral standard stars. An intensity ratio of 0.5–0.7 (primary brighter) at 1600 Å is compatible with the data.

Subject headings: analytical methods — stars: binaries — stars: individual (AO Cassiopeiae) — ultraviolet: spectra

1. INTRODUCTION

AO Cas, a short-period ($3^d.52$), double-lined spectroscopic binary, is a well observed O-star system [O9 III: (n), Walborn 1973]. The orbital elements were recently re-evaluated by Stickland & Lloyd (1988) using spectra from the *International Ultraviolet Explorer Satellite* (*IUE*). The ellipsoidal light curve of the system has been modeled to derive the inclination, masses, and radii (Wood 1963; Hutchings & Hill 1971; Schneider & Leung 1978). In most of these studies, the system is found to be semidetached and the primary star, while less massive, is more luminous than the secondary. For example, Wood and Hutchings and Hill find mass ratios of $q = M_s/M_p = 1.21$ and 1.23, respectively (secondary more massive), while finding Δm (λ4400) = 0.97 and 0.73 (primary brighter). Schneider & Leung by contrast find that $q = 1.19$, but $\Delta m = -0.21$ (secondary brighter). Their result contradicts the spectroscopic finding that the secondary lines are much weaker than those of the primary.

The temperatures of the two stars are poorly determined. Hutchings & Hill find $T_{\rm eff}$ = 39,000 K and 36,000 K for the polar temperatures of the primary (more luminous) and secondary stars, respectively, while Schneider & Leung (1978) find temperatures of 34,700 and 35,033 K for the same two stars. Conti & Alschuler (1971) suggest that the secondary is somewhat hotter than the primary based on the ratio of He II to He I line strengths in their classification spectra.

In a previous paper (Gies & Wiggs 1991), we used *IUE* spectra of the photospheric lines of AO Cas to derive a mass ratio $q = 1.47 \pm 0.08$ by means of cross-correlating a single-lined phase spectrum with the other UV spectra. A line depth ratio of 0.66 was also derived from this data (i.e., the intensity ratio of the stars assuming similar temperatures, with the primary being more luminous). Because the temperatures of the stars are uncertain, the consequences for a model with a hotter secondary were discussed; for example, a temperature increase of 3000 K results in a secondary 17% smaller in diameter.

It is desirable, therefore, to have a way of independently estimating the spectral types and temperatures of the individual stars of AO Cas. In a previous paper by one of us (Bagnuolo & Kamper 1990) several interferometry methods to separate the spectra of binary stars were discussed. For very close binaries like AO Cas use of these techniques will not be feasible until the construction of long baseline optical interferometers, such as has been proposed by McAlister, Bagnuolo, & Hartkopf (1990). An alternative method, using tomography algorithms for spectral separation, will be explored in the remainder of this paper.

There were several reasons for using UV data for AO Cas. In the first place, the data from Gies and Wiggs had good temporal and spectral coverage, and a cross-correlation analysis indicated clearly the presence of numerous secondary photospheric lines. Generally speaking, in the UV there are new sets of indicators for spectral typing of O stars, analogous to the original rather small set of lines in the visual (e.g., He I λ4471, He II $\lambda\lambda$4200, 4542, 4686, Hδ and Hγ). Furthermore the UV photospheric lines form in higher excitation transitions than the optical lines and thus are less prone to contamination from circumstellar emission components. Observations in the visual will provide some complementary data, and we intend to make such observations with the new CHARA 1 m spectroscopic facility currently under construction (Bagnuolo et al. 1990).

2. OBSERVATIONS

The ultraviolet spectra were gathered from the *IUE* Regional Data Analysis Facility in Boulder. A journal of observations and details of the processing of the *IUE* data are given in the previous paper by Gies & Wiggs (1991). Data were extracted in the vicinity of N V λ1240, S IV λ1400, C IV λ1550, He II λ1640, and N IV λ1718, the features described in Gies & Wiggs (1991). For this tomographic analysis, we selected the six spectral regions used by Gies and Wiggs for their cross-correlation study. Gray-scale image depictions of the orbital phase changes in each of these regions shows clearly the photospheric velocity patterns of both stars. The UV spectra were smoothed to reduce noise by convolving the spectra with a Gaussian function with a FWHM = 3 pixels (0.15 Å). The spectra were transformed to a uniform, heliocentric velocity grid, and the velocity registration of each spectrum was altered so that the positions of the interstellar lines matched their positions in a mean global spectrum. The wavelength scale ranges from 0.0465 Å pixel^{-1} (region 1) to 0.0573 Å pixel^{-1} (region 6).

3. TOMOGRAPHY ALGORITHMS

Tomography is mainly known for its medical applications (Barrett & Swindell 1981), but has also been used in diverse applications in astronomy (e.g., Bracewell 1956; Marsh & Horne 1988). In the current context of separating the spectra of a binary star, we can imagine a luminous "object" two pixels thick by n pixels long, where n is the number of pixels per spectrum (or two $1 \times n$ spectral "objects" bonded together). Due to the radial velocity differences of the stars, a number of view angles for tomography are generated in which parallel rays traverse the object and impinge on a detector, producing the observed spectra at a given epoch. Unlike the case for medical tomography, we have restricted view angles and cannot arbitrarily look around the object (although knowing the average intensity of the stars is equivalent to a look along the long axis of the object). Furthermore, the object is not neatly terminated at either end. On the other hand, compared to medical imaging, where typically a square $n \times n$ object is imaged, the binary star case has far fewer points and is more mathematically overdetermined by the data.

A variety of techniques have been tried for tomographic image reconstruction (Brooks & Di Chiro 1976), of which the ILST (iterative least squares technique) seemed the most promising for our application. The general formulation of this algorithm is as follows. Let there be $M = nm$ total measurements, where m is the number of projections, i.e., data sets of n pixels of a general two dimensional object $f(x, y)$ in which f_i represents the intensity of the ith pixel of the object. For a medical tomography case the total number of pixels of the object is $N = n \times n$. Then the intensity of the jth "ray-sum" (a pixel of the set of data) is given by

$$p_j = \sum_{i=1}^{N} W_{ij} f_i , \tag{1}$$

where W_{ij} is the weighting factor that represents the contribution of the ith cell to the jth ray-sum, p_j. Let f_i^q be the qth iteration of the estimated intensity, and for each iteration:

$$\Delta f_i \equiv f_i^{q+1} - f_i^q = \delta \frac{\sum_{l=1}^{m} [W_{il}(p_l - \sum_{k=1}^{N} W_{kl} f_k^q)]}{\sum_{l=1}^{m} W_{il}^2} . \tag{2}$$

That is, we take the set of all rays that include a given cell i and compute the difference between the observed ray intensities and the computed ones using the intensity estimates of the previous iteration. The sum of the differences, weighted appropriately, allows an improved estimate of the intensity at i. The damping factor δ was originally introduced by Goitein (1972), because the original version of the algorithm by Bracewell (1956) often did not converge. Goitein's damping factor was given by a least-squares criterion, but in practice, it was found (Brooks & Di Chiro 1976) that any reasonable choice of a convergent δ gave essentially the same result. In our reconstructions $\delta = 0.3$–0.8 reached a satisfactory convergent solution.

In order to apply this general formulation to the specific case of binary star spectra, we note first that the "object" has dimensions $2 \times n$, where $f_{1,i}$ and $f_{2,i}$ represent the spectra of the primary and secondary, respectively, and i ranges from 1 to n, the length of the spectrum. A further simplication results from setting $W_{ij} = 0$ or 1 only, which provides increased computation speed with little degradation in resolution. Then:

$$\Delta f_{1,i} = \delta \times \frac{\sum_{k=1}^{m} p_{k,i} - (f_{1,i} + f_{2,i+s_k})}{m} , \tag{3a}$$

$$\Delta f_{2,i} = r\delta \times \frac{\sum_{k=1}^{m} p_{k,i-s_k} - (f_{1,i-s_k} + f_{2,i})}{m} , \tag{3b}$$

where $p_{k,i}$ is the ith pixel of the kth binary spectrum (shifted to the velocity frame of the primary star), and s_k is the radial velocity shift of secondary spectrum relative to primary for the kth spectrum. The initial spectra can be either flat or a single-lined spectrum; the spectrum assumed for the secondary is scaled by the assumed intensity ratio r. In general, the reconstructed spectra exhibited little change after 50 iterations, which took $\sim$15 s on a 80386 machine (for $n \approx 500$ pixels and $m = 16$ projections).

A number of simulations were done to test the effectiveness of our version of the ILST algorithm for spectral separation. Figure 1 shows the result for an artificial binary star made up of α Lyr and δ Aql spectra in the 5200 Å region, generously provided by Kamper (1990). Figure 2 shows the spectral separation of a "binary" with a single spectral line in each star (with different widths and depths) for for S/N = 50. (Appropriate noise was generated by a random Gaussian generator, scaled to the square root of the number of "photons" per pixel.) In both figures it can be seen that a good spectral separation was obtained. In Figure 2 the S/N of the separated spectra, particularly the primary, has improved compared to the individual composite spectrum shown. Of course, we use the data from m spectra, not just one, and thus in principle the S/N should improve. Imagine separating two spectra that (say)

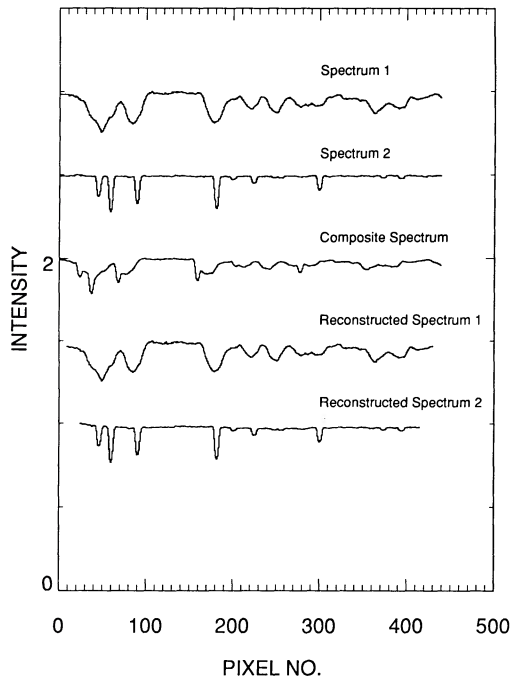

FIG. 1.—Individual spectra recovered from a test composite spectrum made up of δ Aql and α Lyr. Sixteen sets of data were generated, with the spectral shifts of the stars going from 0 to 15 and 0 to -15 pixels, respectively. *Top*: individual spectra (2) of the stars. *Center*: the 8th data set showing composite spectrum. *Bottom*: separated spectra (2) by ILST algorithm. Spectra offset by 0.5 unit in intensity.

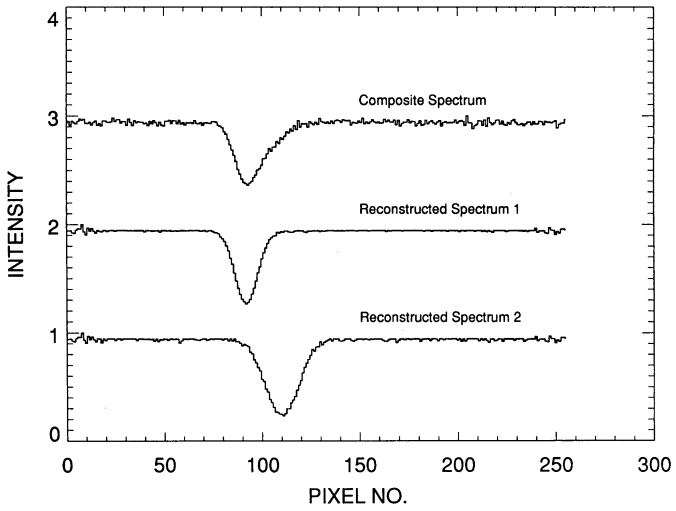

FIG. 2.—Simulated binary spectra for an isolated Gaussian "line." The line in the primary has $\sigma = 5.657$, depth of 0.7 continuum, and centered at pixel 92, while the line from the secondary has $\sigma = 8.660$, depth 0.8, centered at pixel 110. The intensity ratio is 0.4. *Top*: the 8th data set showing composite spectrum for S/N = 50. *Bottom*: the two separated spectra from 16 data sets uniformly spaced in relative radial velocity. Note that the intensity of the secondary spectrum has been normalized.

had lines that did not overlap for a binary with no radial velocity changes. In this ideal case each spectrum would improve in S/N as the square root of the number of spectra, since the spectra could be directly added with no pixel shifts. We expect a similar improvement, although not quite this good, for realistic cases. We also expect that the S/N of the secondary should vary roughly as the intensity ratio, r. We intend to present a separate account of the simulations (Bagnuolo 1991), but it is evident that good spectral separations can occur provided that the binary has an adequate spectral radial velocity shift ($\sim$30% of the FWHM of the photospheric lines, depending on S/N), the spectra have good coverage of the orbit and S/N > 20, and that the spectral region to be reconstructed avoids large spectral lines at the edges. In the AO Cas data discussed in the next section all these conditions are met, especially the radial velocity separation.

4. PHOTOSPHERIC LINES OF THE STARS

The ILST tomography algorithm was applied to seven sets of data consisting of 16 spectra ranging in length from 312 to 651 pixels. (There were six spectral regions: the fifth and sixth data sets overlapped in wavelength, which provided an additional data set as a check on the reconstructed spectra.) The 16 orbital phases of the observations provided good coverage of the spectroscopic orbit. The radial velocities of primary and secondary in each spectrum were taken from the results of Gies & Wiggs (1991) and rounded to the nearest pixel for use in the tomography algorithm. The maximum and minimum radial velocities in pixels for the primary were 20 and -22 pixels; for the secondary, 10 and -18 pixels. For each set of data the 16 spectra were shifted using the radial velocities so that the primary lines in each were aligned (at the same pixel locations). Missing data at either end of the spectra due to the shifts were padded with values of the closest data points. (The seven data sets were originally chosen to not have major spectral features at either end of the spectrum.) The ILST algorithm was then applied, as in equation (3), and the initial spectra assumed for the primary and secondary (scaled in intensity) were that of the eighth data set, which is single-lined (small radial velocity shift between the components). It was found that virtually identical results were obtained by starting from two flat spectra for primary and secondary, but solutions took $\sim$30 more iterations to converge.

The largest uncertainty in the relative velocities of the stars is due to the radial velocity amplitude of the secondary, because that of the primary is well determined. We have run a series of reconstructions for spectral region 2 with the radial velocity amplitude of the secondary varying from 0.6 to 1.4 times its estimated. value. Only minor changes were noted in the spectra. The main reason for this is that the radial velocity amplitude of the primary is $\sim$1.5 times larger than that of the secondary, and thus an error of even 25% in the secondary velocity amplitude translates into an error of only 10% in relative (primary minus secondary) velocity amplitude. Furthermore, the maximum velocity shift in pixels between the components is $\sim$34 pixels, compared to line widths of $\sim$15–30 pixels and an error of 3.4 pixels for a 25% error in secondary velocity amplitude. Because the line width is larger than the errors, the reconstructed lines should have only minor changes.

A final caveat concerns the possible phase dependence of the spectra of the stars. The reconstructed spectrum will be close to an average of the lines over all the input phases, and if these are well distributed about the orbit, the reconstructed spectrum will be close to that of an average spectrum of the star. Because of the uniform phase distribution of our data, we do not expect this to be a major problem with AO Cas. However, if observations are skewed to certain phases, we would expect to get spectra that are not representative of the average over the star. For example, because of temperature variations over the star, spectral type becomes a function of orbital phase. An analysis done by us, based on the model by Gies & Wiggs (1991), shows that the temperature effects in the primary are dominated by tidal distortion, not irradiation from the secondary. The temperature at latitude 29°, approximately the disk center for our line of sight, varies by about $\pm$1000°, and the hemisphere averaged temperature would vary by a much smaller amount. Second, because of tidal effects, we expect some distortion in the star shapes. According to the model of Gies & Wiggs (1991) the AO Cas stars are well separated, and the secondary suffers little tidal distortion. The primary, however, almost fills its Roche lobe and is significantly distorted. The ratio of the minimum to maximum equatorial diameters of the star is $\sim$0.80. The primary is $\sim$21% larger in areas seen "broadside" at phases 0.25 or 0.75 than at phases 0.0 or 0.5. We would thus expect to see primary spectral lines that are somewhat broader at such quadrature phases. Again, the results of the tomographic reconstruction will reflect the phase distribution of the data.

The separated individual spectra of the two stars are given in Figures 3–8. These results are from 150 iterations, although little change was noted after 50 iterations. An intensity ratio of $r = 0.66$ was assumed, based on an analysis described below. Thirty-two pixels at either end were omitted from these reconstructed spectra to avoid edge effects. Spectral classifications of the two stars for each spectral region were done, based upon standard spectra in the *International Ultraviolet Explorer Atlas of O-Type Spectra from 1200 to 1900 Å* (Walborn, Nichols-Bohlin, & Panek 1985) hereafter referred to as "the O-star

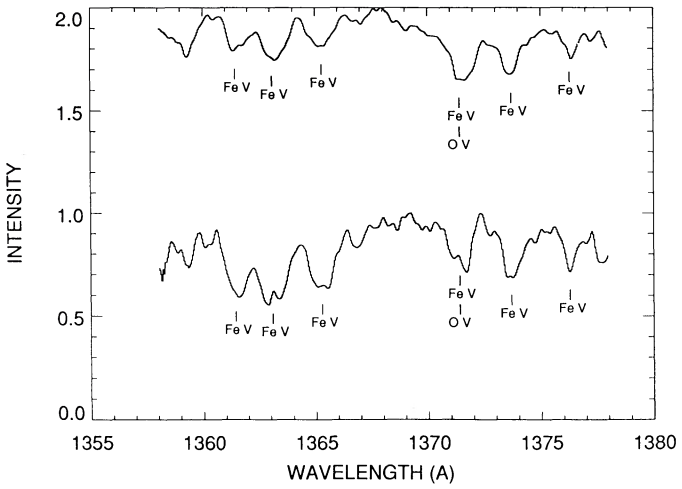

FIG. 3.—Spectra of the primary (*top*) and secondary (*below*) stars of AO Cas, from tomography of 16 *IUE* spectra, in region 1 (1360–1378 Å). Both spectra are recitified to unit continuum. For clarity the primary spectrum is offset by one unit.

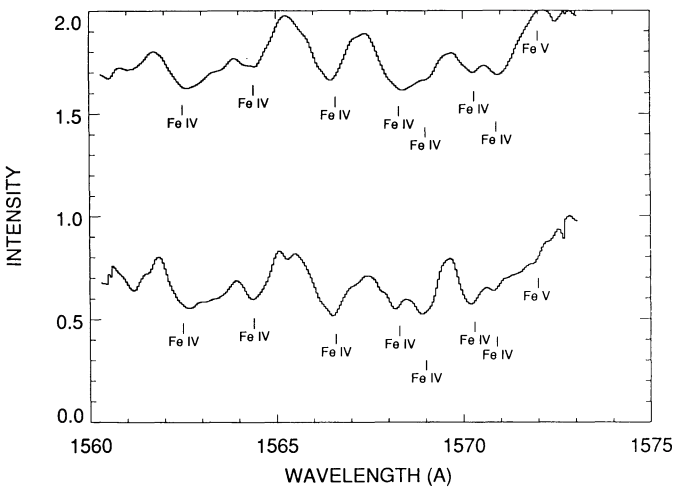

FIG. 5.—Spectra of the primary and secondary stars of AO Cas in region 3 (1560–1573 Å).

Atlas," and the spectral sequence of Walborn & Panek (1984). Additional line identifications were derived from Bruhweiler, Kondo, & McCluskey (1981) and McCluskey & Kondo (1981). To better facilitate comparison with the O-star Atlas, plots were also made with the x-axes compressed to match the aspect ratio of spectra in the Atlas. The following are the results of these classifications:

Region 1. 1360–1378 Å (Fig. 3).—This region is dominated by Fe v lines ($\lambda\lambda$1361, 1363, 1366, 1371, 1373, 1376) which strengthen from B0 to O6. The pseudo-continuum "hill" at 1368 Å strengthens from O9.5 through O7.5 and also appears stronger in giants than dwarfs.

The rather weak Fe v line strength of the primary ($\approx$10%–20% of continuum) and the weakness of the 1368 Å feature suggest that it is a star like HD 48434 (B0 III) or possibly HD 189957 (O9.5 III) in the O-star Atlas.

The relative strength of the Fe v lines in the secondary ($\approx$20%–35% of continuum) compared to the primary thus suggests that the secondary is hotter. (In region 3, by contrast, the Fe IV lines in the secondary are weaker than the primary.) The best fit to the secondary is O7.5 V–O8.5 V (HD 152590, HD 101413, and δ Ori). The relative weakness of the λ1368 feature suggests that the secondary is luminosity class V rather than III.

Region 2. 1412–1438 Å (Fig. 4).—Fe v, C III lines are prominent in this region. The main features are the Fe v lines at $\lambda\lambda$1430, 1429, the C III lines at $\lambda\lambda$1426, 1428, and the Fe v blend around λ1420. The Fe v λ1430 line strengthens compared to C III $\lambda\lambda$1426, 1428 from B0 through O5, and appears to be somewhat stronger in giants than dwarfs. The Fe v λ1420 blend strengthens relative to surroundings from B0 to about O7.5.

Based on these two criteria, the primary spectrum is matched best with O9.5 III (HD 189957), and to a lesser extent B0 III (HD 48434) and O9 III (HD 193443). The secondary is best matched by O8 V (HD 101413) and O8.5 V (δ Ori). The relative weakness of Fe v λ1430 in the secondary definitely rules out a fit with a star earlier than O7.5.

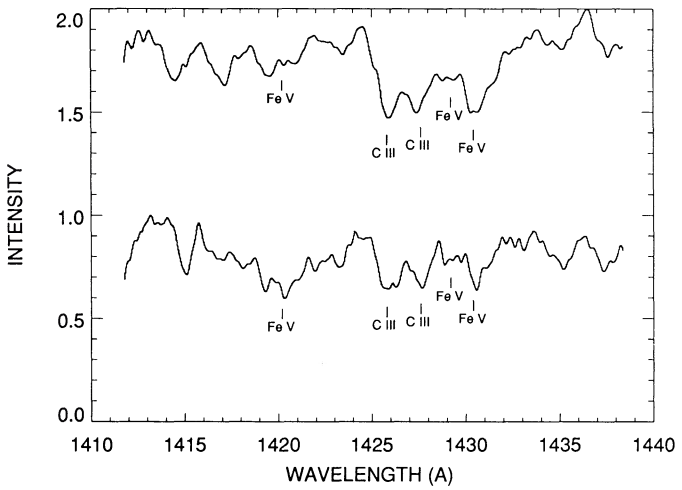

FIG. 4.—Spectra of the primary and secondary stars of AO Cas in region 2 (1412–1438 Å).

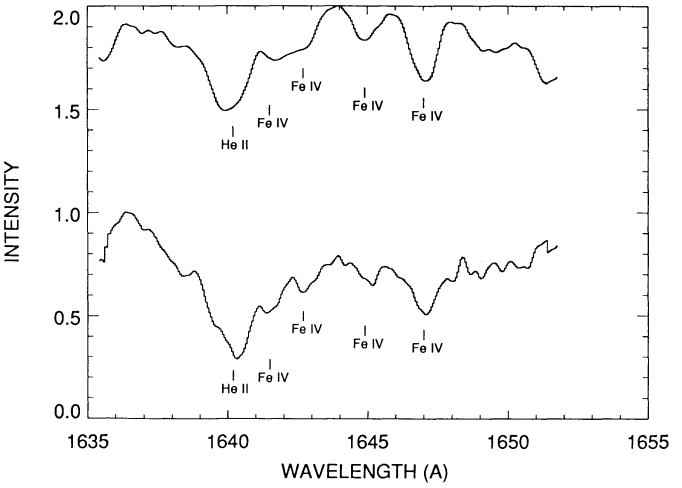

FIG. 6.—Spectra of the primary and secondary stars of AO Cas in region 4 (1635–1652 Å).

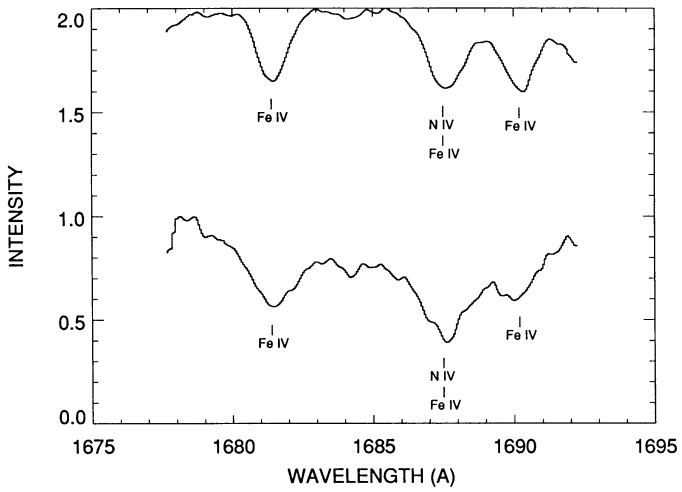

FIG. 7a

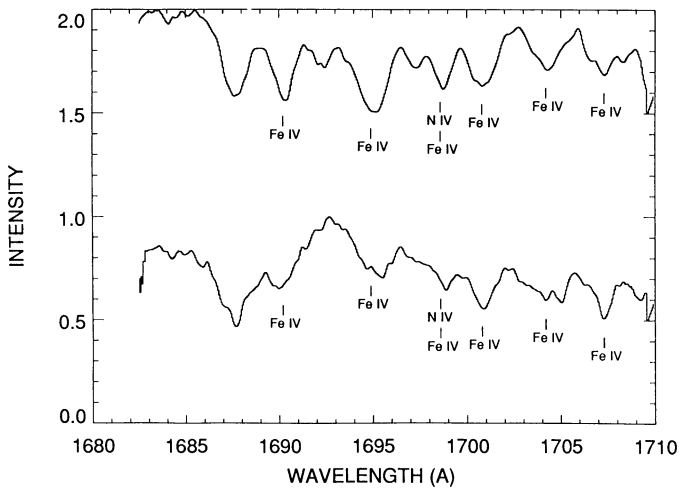

FIG. 7b

FIG. 7.—(*a*) Spectra of the primary and secondary stars of AO Cas in region 5 (1677–1689 Å). (*b*) Spectra of the primary and secondary stars of AO Cas in region 5 (1685–1709 Å). Note overlap with previous spectrum, and also similarity of reconstructed features from the two data sets.

Region 3. 1560–1573 Å (Fig. 5).—Dominant Fe IV lines in this region are found at λλ1563, 1564, 1566, 1568–9, 1570–1. These lines generally tend to weaken from O9 through O6. A weak Fe V line at λ1572 possibly appears in the secondary. Fe IV lines in the primary star are generally stronger than in the secondary. As noted in the remarks for region 1, the relative line strengths indicate that the primary is cooler than the secondary.

The best fits to the primary spectrum are O9.5 III (HD 189957) and O9.5 V (μ Col). The best fit to the secondary is O8 V (HD 101413), and it seems very unlikely that the secondary can be as late as O9, because in stars of that class (e.g., 10 Lac) the Fe IV lines are much stronger.

Region 4. 1635–1652 Å (Fig. 6).—This region contains Fe IV lines and the prominent He II line at λ1640. The Fe IV lines of the primary are generally stronger than those of the secondary, but the primary's He II line is at least as strong in that of the secondary. The ratio of lines Fe IV:He II indicates a hotter secondary, because the line strength of the latter changes very slowly with spectral type. There do not appear to be any noticeable luminosity effects in this waveband.

The best match to the primary is B0 III (HD 48434), based on the Fe IV:He II line ratios, particularly λ1647:λ1640. The best matches to the secondary are O8 V (HD 101413) and O8.5 V (HD 46149).

Region 5. 1677–1709 Å (Figs. 7*a* and 7*b*).—This region contains primarily Fe IV and N IV lines. As in regions 3 and 4, the Fe IV lines in the secondary are uniformly weaker than the primary, except λ1688 which contains a N IV line. (Compare the line ratios Fe IV λ1690, 1695:N IV λ1688, which are weaker in the secondary.) The "peak" in the secondary spectrum at λ1692 is not seen in the primary.

The best match for the primary is O9 III (ι Ori, HD 193443). The secondary is best fitted by O8 V (HD 101413), and to a lesser extent O8.5 V (HD 46149).

Region 6. 1743–1767 Å (Fig. 8).—This region contains two prominent N III lines, and several Fe IV lines. The unidentified line at λ1758 appears weak for stars earlier than O9 III or O8.5 V, and stronger for stars later than these. The Fe IV λ1765 line grows stronger from O7.5 to B0. No noticable luminosity effects appear in this waveband.

The best match to the primary spectrum is O9 III (HD 193443); next, B0 III (HD 48434). The best match to the secondary spectrum is O8 V (HD 101443); next best are O7.5 V (HD 152590) and O8.5 V (HD 46749).

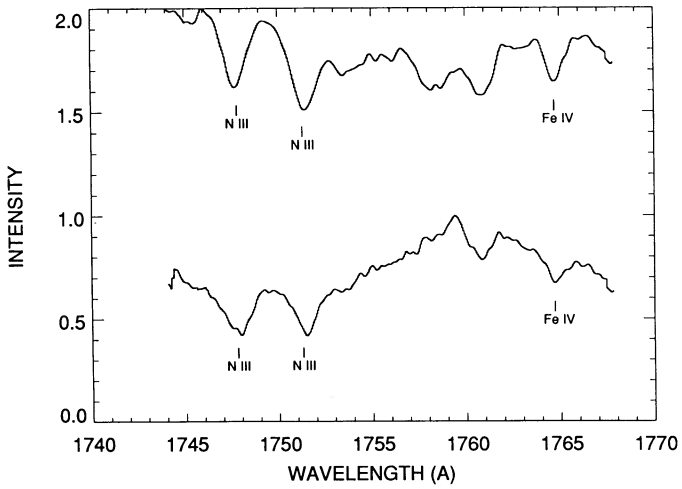

FIG. 8.—Spectra of the primary and secondary stars of AO Cas in region 6 (1743–1767 Å).

The best overall estimate of the spectral types of the primary and secondary stars, are O9.5 III and O8.1 V, respectively, based on an unweighted average for the six regions. (The estimated spectral types for the primary in the six regions are: O9.75, O9.5, O9.5, B0.0, O9.0, and O9.33. For the secondary the types are O8.0, O8.25, O8.0, O8.25, O8.25, and O8.0. In these estimates the stars mentioned as "best fit" were weighted 1.0, and those mentioned as "next best" were weighted 0.5.)

Finally, the He II λ1640 line can be used for an estimate of the continuum intensity ratio of the stars. This line has several advantages for this determination. It is the deepest line in our sample of data, it is relatively isolated, and furthermore, it is known to vary only slowly with spectral type. Provided that lines of either star do not reach zero intensity, there is an

ambiguity in the reconstructed spectra from tomography. (One could satisfy the reconstruction equations by taking a strip of uniform intensity from the bottom of one spectrum and adding it to the other.) However, if the assumed intensity ratio, r, of the overall intensities of the spectra is too low, the deepest reconstructed lines of the secondary will attempt to go below zero. In particular, the reconstructed He II line goes to zero ("tries" for a nonphysical solution) for $r < 0.3$. Assuming that the He II line is equal for both stars requires that $r = 0.5$ to 0.7. The line strengths of the reconstructed spectra are thus reasonably compatible with the value of $r = 0.66$ derived by Gies & Wiggs (1990) from a cross-correlation analysis, and this value was therefore used in the algorithm to produce the reconstructed spectra.

5. CONCLUSIONS

Our results show that the secondary of AO Cas is ~ 1.4 spectral subclasses earlier than the primary. According to the temperature–spectral type calibration of Howarth & Prinja (1989) temperatures of $\sim 32{,}000$ and 36,000 K are indicated for the primary and secondary, respectively. Our results thus support the contention by Conti & Alschuler (1971) that the secondary is the hotter star. The temperature difference between the components cannot be much greater than 4000° because the photometric light curve becomes difficult to fit with such a smaller secondary (Gies & Wiggs 1991). Furthermore, a greater temperature difference would lead to a measurable color difference in the light curves. (Assuming 32,000 and 36,000 K for primary and secondary respectively leads to a difference at the conjunctions of 0.007 in $B-V$.) The data are consistent with an intensity ratio for the stars of 0.5–0.7 in the UV (1600 Å), the same range used by Gies and Wiggs, based on optical line depth ratios. In general, we hope that the determination of temperatures, radii, and other physical parameters of close O-star binaries such as AO Cas will help to elucidate the evolution of such systems.

Finally, we have shown how the application of a simple tomographic algorithm can produce useful information on the individual spectral types and intensity ratios of binary stars. It should also be possible to better determine the rotational velocities of the individual stars. This algorithm can also be used to enhance the spectral separation obtained by other means such as interferometry or eclipses provided that the intensity ratio at each epoch can be estimated.

We wish to acknowledge K. Kamper, T. Meylan, P. Benkeser, W. Hartkopf, H. McAlister, and an anonymous reviewer for useful criticism. One of us (W. G. B.) has been partially supported by NSF grants AST 88-06993 and AST 89-16110. D. R. G. gratefully acknowledges the financial support of the NASA Astrophysics Data Program Grant NAG 5-1218.

REFERENCES

Bagnuolo, W. G., Jr. 1991, in preparation.
Bagnuolo, W. G., Jr., Furenlid, I. K., Gies, D. R., Barry, D. J., Russell, W. H., & Dorsey, J. F. 1990, PASP, 102, 604
Bagnuolo, W. G., Jr., & Kamper, K. W. 1990, PASP, 102, 351
Barrett, H. H., & Swindell, W. 1981, Radiological Imaging, Vol. 2 (New York: Academic), 375
Bracewell, R. N. 1956, Australian J. Phys., 9, 198
Brooks, R. A., & Di Chiro, G. 1976, Phys. Med. Biol., 21, 690
Bruhweiler, F. C., Kondo, Y., & McCluskey, G. E. 1981, ApJS, 46, 255
Conti, P. S., & Alschuler, W. R. 1971, ApJ, 170, 325
Gies, D. R., & Wiggs, M. S. 1991, ApJ, 375, 321
Goitein, M. 1972, Nucl. Instr. Meth., 101, 509
Howarth, I. D., & Prinja, R. K. 1989, ApJS, 69, 527
Hutchings, J. B., & Hill, G. 1971, ApJ, 167, 137
Kamper, K. W. 1990, private communication
Marsh, T. R., & Horne, K. 1988, MNRAS, 235, 269
McAlister, H. A., Bagnuolo, W. G., Jr., & Hartkopf, W. I. 1990, Amplitude and Intensity Spatial Interferometry, ed. J. B. Breckinridge (Proc. SPIE, 1237), 22
McCluskey, G. E., & Kondo, Y. 1981, ApJ, 246, 464
Schneider, D. P., & Leung, K.-C. 1978, ApJ, 223, 202
Stickland, D. J., & Lloyd, C. 1988, Observatory, 108, 174
Walborn, N. R. 1973, AJ, 78, 1067
Walborn, N. R., Nichols-Bohlin, J., & Panek, R. J. 1985, International Ultraviolet Explorer Atlas of O-Type Spectra from 1200 to 1900 Å, NASA RP, 1155
Walborn, N. R., & Panek, R. J. 1984, ApJ, 286, 718
Wood, F. B. 1963, in Basic Astronomical Data, ed. K. Aa. Strand (Chicago: Univ. of Chicago Press), 370